Article

Fighting against fast speckle decorrelation for light focusing inside live tissue by photon frequency shifting

Jiamiao Yang, Lei Li, Jingwei Li, Zhongtao Cheng, Yan Liu, and Lihong V. Wang

ACS Photonics, **Just Accepted Manuscript** • DOI: 10.1021/acsphotonics.0c00027 • Publication Date (Web): 26 Feb 2020

Fighting against fast speckle decorrelation for light focusing inside live tissue by photon frequency shifting

Jiamiao Yang,[†] Lei Li,[†] Jingwei Li,[†,‡] Zhongtao Cheng,[†] Yan Liu,[†] and Lihong V. Wang*[,†]

[†]*Caltech Optical Imaging Laboratory, Andrew and Peggy Cherng Department of Medical Engineering, Department of Electrical Engineering, California Institute of Technology, Pasadena, California 91125, USA*

[‡]*Present address: Centre for Optical and Electromagnetic Research, Chinese National Engineering Research Center for Optical Instruments, Zhejiang University, Hangzhou 310058, China*

**E-mail: LVW@caltech.edu.*

Light focusing inside live tissue by digital optical phase conjugation (DOPC) has drawn increasing interest due to its potential biomedical applications in optogenetics, microsurgery, phototherapy, and deep-tissue imaging. However, fast physiological motions in a live animal, including blood flow and respiratory motions, produce undesired photon perturbation and thus inevitably deteriorate the performance of light focusing. Here, we develop a photon-frequency-shifting DOPC method to fight against fast physiological motions by switching the states of a guide star at a distinctive frequency. Therefore, the photons tagged by the guide star are well detected at the specific frequency, separating them from the photons perturbed by fast motions. Light focusing was demonstrated in both phantoms in vitro and mice in vivo with substantially improved focusing contrast. This work puts a new perspective on light focusing inside live tissue and promises wide biomedical applications.

Keywords: Wavefront shaping; Digital optical phase conjugation; Dynamic scattering medium; Guide star; Spatial light modulator; Lock-in detection; Angular-spectrum model.

INTRODUCTION

Focusing light inside biological tissue is crucial to abundant applications, such as deep-tissue imaging, optical tweezing, optogenetics, microsurgery, and phototherapy. However, biological tissue with a heterogeneous refractive index distribution scatters light, which causes photons to diverge from the original paths. In consequence, it is a challenge to achieve optical focusing deep inside biological tissue, limiting the aforementioned applications to shallow regions (less than 1 mm deep in biological tissue). The emerging wavefront shaping technologies provide a solution to realizing light focusing deep inside biological tissue. By shaping the wavefront of the incident light, the wave disturbance induced by the refractive-index inhomogeneity is compensated for to reconstruct a focus inside tissue. Wavefront shaping technologies can be classified into three categories based on the methodologies to recognize the optimal wavefront: the transmission matrix method[1–4], the feedback-based method[5–8], and the optical phase conjugation (OPC) method[9–21]. Particularly, digital OPC (DOPC) arose as a compelling method with the characteristics of high focusing speed and high focusing contrast by measuring the tagged photons' wavefront directly. DOPC is capable to realize light focusing deep inside biological tissue with a controllable guide star, including fluorescence markers[22,23], focused ultrasound[16,17,24,25], kinetic targets[15,26], microbubbles[27], and magnetic particles[28,29].

For *in vivo* applications, however, fast physiological motions, including blood flow and respiratory motions, perturb photons simultaneously with the guide star tagging during the DOPC process[21]. This perturbation generates competition between the guide star with respect to the photons tagging and the fast physiological motions, which unavoidably deteriorates the quality of light focusing. To mitigate the influence of the fast physiological motions, high-speed DOPC systems were developed to minimize the field perturbation during the process of DOPC[10,30,31]. However, due to the limited speeds of cameras, data transfer, data processing, and spatial light modulators (SLMs), the focusing contrast promoted by this method is inadequate for biomedical applications.

Here, we propose a photon-frequency-shifting DOPC (PFS-DOPC) method to fight against fast physiological motions. By switching the states of a guide star at a distinctive frequency, the photons tagged

by the guide star are modulated at this specific frequency. In contrast, the fast physiological motions disturb the light field randomly over time. Thus, by selecting photons at the specific frequency through essentially lock-in detection, the perturbation caused by fast physiological motions is greatly suppressed. To verify the superior performance of PFS-DOPC, we demonstrated light focusing in both tissue phantoms *in vitro* and mice *in vivo* and obtained 18-fold and 12-fold enhancement of the peak-to-background ratio (PBR) of optical foci, respectively.

RESULTS

Principle of PFS-DOPC

Figure 1(a) illustrates the principle of focusing light inside live tissue using binary-phase DOPC[30,32]. A controllable guide star, embedded in the tissue, tags the photons passing through it by changing their properties, including amplitude, phase, and polarization. Thus, the detected optical field of the scattered light outside the tissue has been transformed from E_1 to E_2 because of the state changing of the guide star [Figs. 1(b) and 1(c)]. To probe the field difference ΔE between E_1 and E_2, a reference beam is introduced to interfere with the scattered light exiting the tissue [blue indented filled arrow in Fig. 1(a)]. Two holograms, I_{holo1} and I_{holo2}, are captured by a camera when the reference beam interferes with E_1 and E_2, respectively. Subsequently, a playback beam with an optical field of E_{playback} [black open sharp arrow in Fig. 1(a)] is achieved by modulating the reference beam with a binary conjugated phase map of ΔE via an SLM located at the camera's conjugate position. The binary conjugated phase map of ΔE is calculated by

$$\varphi_{\text{SLM}}(x,y) = \begin{cases} 0, & \text{if } I_{\text{holo1}}(x,y) \geq I_{\text{holo2}}(x,y) \\ \pi, & \text{if } I_{\text{holo1}}(x,y) < I_{\text{holo2}}(x,y). \end{cases} \quad (1)$$

As shown in Fig. 1(d), once E_{playback} propagates back inside the tissue, a time-reversed focus is formed at the position of the guide star (for details, see Supporting Information S1).

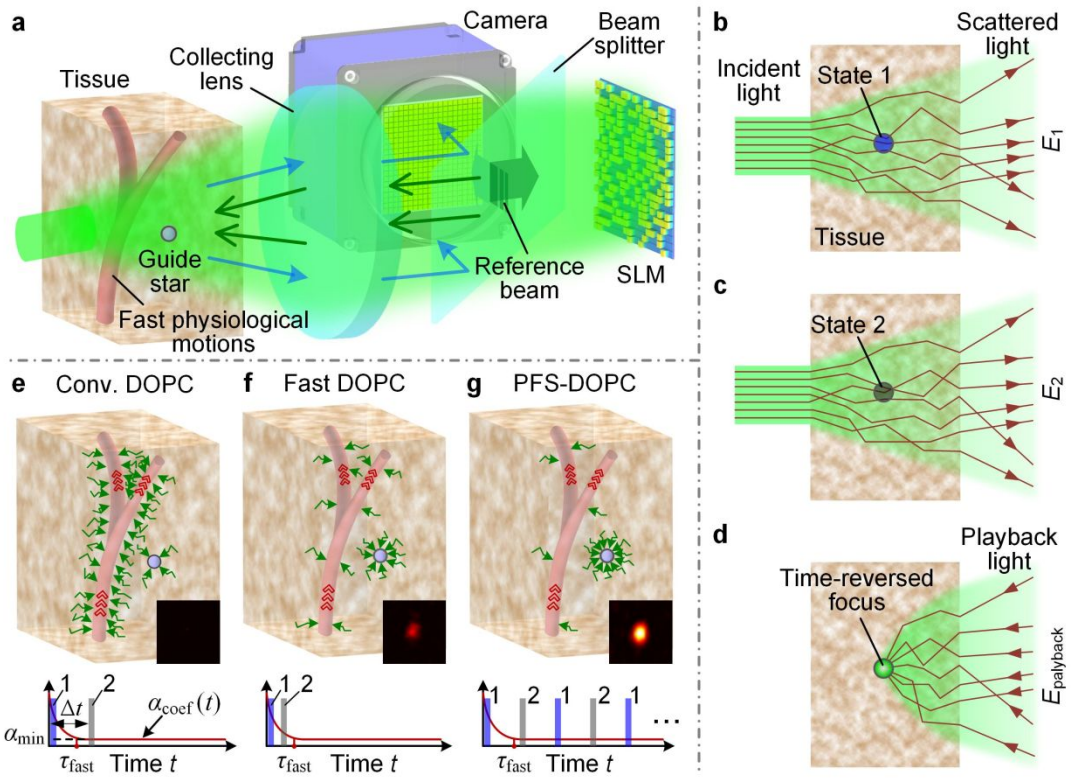

Figure 1. Principle and schematic of PFS-DOPC. (a) Principle of focusing light inside tissue using binary-phase DOPC. (b–d) Schematic of light focusing inside tissue on a guide star. The detected optical field is transformed from E_1 to E_2 due to the changes of the guide star state. $E_{playback}$ is produced to form a time-reversed focus on the guide star. (e–g) Comparison of light focusing inside live tissue between conventional (conv.) DOPC, fast DOPC, and PFS-DOPC when fast physiological motions exist. The bottom panels in (e–g) illustrate the hologram acquisition strategy of each method, where the red line is the speckle correlation coefficient $\alpha_{coef}(t)$ of the tissue as a function of time t, and τ_{fast} is the decorrelation time caused by fast physiological motions.

However, fast physiological motions, such as blood flow and respiratory motions, can also induce an optical field change. If the time interval Δt between the two acquisitions of the holograms I_{holo1} and I_{holo2} is longer than the decorrelation time τ_{fast} caused by fast physiological motions [Fig. 1(e)], fast physiological motions would contribute a significant component in the measured ΔE. Thus, when $E_{playback}$ propagates back inside the tissue, a large amount of the photons would focus on the tissue with fast motions, creating a bright background and resulting in low focusing quality on the guide star. To minimize ΔE induced by fast physiological motions and enhance the light focusing quality, fast DOPC [Fig. 1(f)] was developed to

reduce Δt to less than τ_{fast} (for details, see Supporting Information S2). However, the shortest DOPC time, including camera exposure, data transfer, data processing, and SLM display, is about 6 ms[30], still limiting the focusing quality in tissue with fast blood flow.

To fight against fast physiological motions, our proposed PFS-DOPC switches the guide star from State 1 to State 2 at a distinctive frequency of f_{mod} for N cycles, as shown in Fig. 1(g). Assuming that the modulation coefficient of the guide star is $M_{\text{GS}}(t)$, the optical field of the photons passing through the guide star is obtained as

$$E_{\text{mod}}(t) = AM_{\text{GS}}(t) \cdot \exp[i(-2\pi f_0 t + \varphi_0)], \tag{2}$$

where t is time, f_0 is the original optical frequency, A and φ_0 are the initial amplitude and phase, respectively. Because $M_{\text{GS}}(t)$ is a periodic function with a fundamental frequency of f_{m}, Eq. (2) can be expanded into a Fourier series:

$$\begin{aligned} E_{\text{mod}}(t) = &\sum_{n=1}^{\infty} AB_{-n}\exp\{i[-2\pi(f_0 - nf_{\text{mod}})t + \varphi_0]\} \\ &+ \sum_{n=1}^{\infty} AB_n\exp\{i[-2\pi(f_0 + nf_{\text{mod}})t + \varphi_0]\} \\ &+ AB_0\exp[i(-2\pi f_0 t + \varphi_0)], \end{aligned} \tag{3}$$

and

$$B_n = f_{\text{mod}}\int_0^{1/f_{\text{mod}}} M_{\text{GS}}(t)\exp(i2\pi n f_{\text{mod}}t)dt. \tag{4}$$

Thus, the frequency of a portion of the photons passing through the guide star is shifted to $f_0 \pm nf_{\text{mod}}$ ($n = 1, 2, 3, \ldots$). By detecting only tagged photons with frequencies of $f_0 \pm f_{\text{mod}}$, the photons tagged by the guide star can be separated from the photons perturbed by fast motions. To measure the wavefront of the tagged photons, a reference beam with a frequency of f_0 is added to generate an interference pattern with the scattered light. Because of the frequency difference between the reference beam and the tagged photons, a beat frequency of f_{mod} exists in the interference pattern. To calculate the wavefront of the tagged photons, $2N$ holograms are recorded with a time interval of $1/(2f_{\text{mod}})$ during N cycles of the beat. The binary phase map φ_{SLM} of the tagged photons is calculated by (for details, see Supporting Information S3)

$$\varphi_{\text{SLM}}(x, y) = \begin{cases} 0, & \text{if } \Delta\bar{I}_{\text{holo}}(x, y) \geq 0 \\ \pi, & \text{if } \Delta\bar{I}_{\text{holo}}(x, y) < 0 \end{cases}, \tag{5}$$

where $\Delta\bar{I}_{\text{holo}}(x,y) = \bar{I}_{\text{holo1}}(x,y) - \bar{I}_{\text{holo2}}(x,y)$, $\bar{I}_{\text{holo1}}(x,y)$ and $\bar{I}_{\text{holo2}}(x,y)$ are the averaged holograms with the guide star in State 1 and State 2, respectively.

Minimizing the impact of the fast physiological motions by PFS-DOPC

When fast physiological motions exist, the optical field $\mathbf{E}_{\text{out}}$ of the scattered light exiting the scattering medium can be decomposed into three components, $\mathbf{E}_{\text{out}} = \mathbf{E}_{\text{G}} + \mathbf{E}_{\text{S}} + \mathbf{E}_{\text{D}}$, where $\mathbf{E}_{\text{G}}$ is the component modulated by the guide star, $\mathbf{E}_{\text{S}}$ is a stable component that does not change during the DOPC process, and $\mathbf{E}_{\text{D}}$ is the fast decorrelation component induced by tissue motions and it varies randomly during this process. Denote the m-th element of $\mathbf{E}_{\text{G}}$, $\mathbf{E}_{\text{S}}$ and $\mathbf{E}_{\text{D}}$ as $E_{\text{G}}^{(m)}$, $E_{\text{S}}^{(m)}$ and $E_{\text{D}}^{(m)}$, respectively. Then, the intensity of the m-th element $I_{\text{holo}}^{(m)}$ of the captured hologram can be written as

$$\begin{aligned} I_{\text{holo}}^{(m)} &= \left(E_{\text{G}}^{(m)} + E_{\text{S}}^{(m)} + E_{\text{D}}^{(m)} + E_{\text{R}}\right) \times \left(E_{\text{G}}^{(m)} + E_{\text{S}}^{(m)} + E_{\text{D}}^{(m)} + E_{\text{R}}\right)^{*} \\ &= E_{\text{G}}^{(m)} E_{\text{G}}^{(m)\,*} + E_{\text{R}} E_{\text{R}}^{*} + E_{\text{S}}^{(m)} E_{\text{S}}^{(m)\,*} + E_{\text{D}}^{(m)} E_{\text{D}}^{(m)\,*} + 2\text{real}\left(E_{\text{G}}^{(m)} E_{\text{S}}^{(m)\,*}\right. \\ &\quad \left. + E_{\text{G}}^{(m)} E_{\text{D}}^{(m)\,*} + E_{\text{G}}^{(m)} E_{\text{R}}^{*} + E_{\text{S}}^{(m)} E_{\text{D}}^{(m)\,*} + E_{\text{S}}^{(m)} E_{\text{R}}^{*} + E_{\text{D}}^{(m)} E_{\text{R}}^{*}\right). \end{aligned} \tag{6}$$

where E_{R} is the optical field of the reference beam.

By averaging the corresponding holograms across cycles and taking the difference between the two averaged holograms, the m-th element of the differential hologram is obtained as

$$\begin{aligned} \Delta\bar{I}_{\text{holo}}^{(m)} &= \frac{\sum_{n=0}^{N}\left[I_{\text{holo}}^{(m)}\big|_{t=t_0+n/f_{\text{mod}}}\right]}{N} - \frac{\sum_{n=0}^{N}\left[I_{\text{holo}}^{(m)}\big|_{t=t_0+(2n+1)/(2f_{\text{mod}})}\right]}{N} \\ &= \frac{\sum_{n=0}^{N}\left[2\text{real}\left(E_{\text{G}}^{(m)} E_{\text{S}}^{(m)\,*} + E_{\text{G}}^{(m)} E_{\text{D}}^{(m)\,*} + E_{\text{G}}^{(m)} E_{\text{R}}^{*} + E_{\text{S}}^{(m)} E_{\text{D}}^{(m)\,*} + E_{\text{D}}^{(m)} E_{\text{R}}^{*}\right)\big|_{t=t_0+n/f_{\text{mod}}}\right]}{N} \\ &\quad - \frac{\sum_{n=0}^{N}\left[2\text{real}\left(E_{\text{G}}^{(m)} E_{\text{S}}^{(m)\,*} + E_{\text{G}}^{(m)} E_{\text{D}}^{(m)\,*} + E_{\text{G}}^{(m)} E_{\text{R}}^{*} + E_{\text{S}}^{(m)} E_{\text{D}}^{(m)\,*} + E_{\text{D}}^{(m)} E_{\text{R}}^{*}\right)\big|_{t=t_0+(2n+1)/(2f_{\text{mod}})}\right]}{N}. \end{aligned} \tag{7}$$

Because the amplitude of E_{R} and $E_{\text{S}}^{(m)}$ are much larger than those of $E_{\text{G}}^{(m)}$, and $E_{\text{D}}^{(m)}$ in our experiments, $E_{\text{G}}^{(m)} E_{\text{S}}^{(m)\,*}$ and $E_{\text{G}}^{(m)} E_{\text{D}}^{(m)\,*}$ are negligible; thus, Eq. (7) can be simplified to

$$\begin{aligned} \Delta\bar{I}_{\text{holo}}^{(m)} &= \frac{\sum_{n=1}^{N}\left[2\text{real}\left(E_{\text{G}}^{(m)} E_{\text{R}}^{*} + E_{\text{S}}^{(m)} E_{\text{D}}^{(m)\,*} + E_{\text{D}}^{(m)} E_{\text{R}}^{*}\right)\big|_{t=t_0+n/f_{\text{mod}}}\right]}{N} \\ &\quad - \frac{\sum_{n=1}^{N}\left[2\text{real}\left(E_{\text{G}}^{(m)} E_{\text{R}}^{*} + E_{\text{S}}^{(m)} E_{\text{D}}^{(m)\,*} + E_{\text{D}}^{(m)} E_{\text{R}}^{*}\right)\big|_{t=t_0+(2n+1)/(2f_{\text{mod}})}\right]}{N}. \end{aligned} \tag{8}$$

Across cycles, $E_{\text{D}}^{(m)} E_{\text{R}}^{*} + E_{\text{S}}^{(m)} E_{\text{D}}^{(m)\,*}$ changes randomly, while $E_{\text{G}}^{(m)} E_{\text{R}}^{*}$ changes periodically following the guide star modulation. Thus, Eq. (8) can be rewritten as

$$\Delta\bar{I}_{\mathrm{holo}}^{(m)} = \frac{2\sum_{n=1}^{N}\left[\mathrm{real}\left(E_{\mathrm{S}}^{(m)}E_{\mathrm{D}}^{(m)*} + E_{\mathrm{D}}^{(m)}E_{\mathrm{R}}^{*}\right)\Big|_{t=t_0+n/f_{\mathrm{mod}}} - \mathrm{real}\left(E_{\mathrm{S}}^{(m)}E_{\mathrm{D}}^{(m)*} + E_{\mathrm{D}}^{(m)}E_{\mathrm{R}}^{*}\right)\Big|_{t=t_0+(2n+1)/(2f_{\mathrm{mod}})}\right]}{N} + 2\left[\mathrm{real}\left(E_{\mathrm{G}}^{(m)}E_{\mathrm{R}}^{*}\right)\Big|_{t=t_0+n/f_{\mathrm{mod}}} - \mathrm{real}\left(E_{\mathrm{G}}^{(m)}E_{\mathrm{R}}^{*}\right)\Big|_{t=t_0+(2n+1)/(2f_{\mathrm{mod}})}\right]. \quad (9)$$

Therefore, the perturbation of the fast physiological motions is minimized by reducing the amplitude of the first term on the right-hand side with a factor of $\sqrt{N}$.

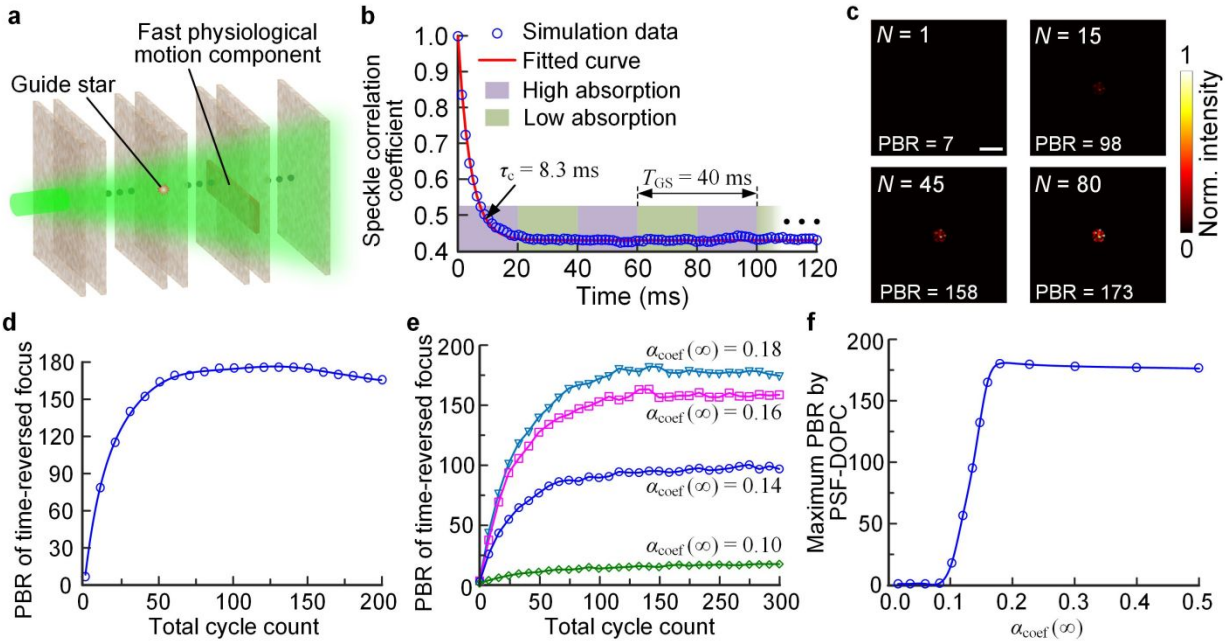

Figure 2. Simulation of the fast tissue motion suppression of PFS-DOPC using an angular-spectrum model. (a) Modeling light propagation inside a dynamic scattering medium. A guide star and a fast physiological motion component were embedded at two different positions inside the scattering medium. (b) Speckle correlation coefficient $\alpha_{\mathrm{coef}}(t)$ as a function of time t. (c) Normalized (Norm.) intensity distribution of DOPC foci with total cycle counts N = 1, 15, 45 and 125, respectively. Scale bar, 100 μm. (d) PBR of the time-reversed focus as a function of the total cycle count N. (e) PBR of the time-reversed focus as a function of the total cycle count N when $\alpha_{\mathrm{coef}}(\infty)$ = 0.18, 0.16, 0.14, and 0.10, respectively. (f) Maximum PBR of the time-reversed focus obtained by the PFS-DOPC as a function of $\alpha_{\mathrm{coef}}(\infty)$.

To verify the performance of PFS-DOPC, we first carried out a numerical simulation based on the angular-spectrum method[21], as shown in Fig. 2. In the simulation, light transmission through a lens was modeled by a lens transmission function $\exp\left[-i\pi(x^2 + y^2)/\lambda f\right]$, where λ is the wavelength and f is the lens focal length. To simulate photon propagation inside a scattering medium, the scattering medium was

divided into multiple layers, and each layer was squeezed into an infinitesimally thin plane with a small distance between two neighboring planes. We gridded each layer and assigned a random number to the refractive index in each grid. Then, we employed the angular-spectrum method to simulate the photon propagation plane by plane. As shown in Fig. 2(a), a guide star and a fast physiological motion component were embedded at two different positions. The light transmittance through the fast physiological motion component was randomly changed with an additional amplitude and phase at each pixel. The decorrelation time caused by the fast physiological motion component was controlled by changing the values of the additional amplitude, the additional phase, and the time interval for each step (for details, see Supporting Information S4). Figure 2(b) shows the speckle correlation coefficient $\alpha_{\mathrm{coef}}(t)$ as a function of time t. Accordingly, the decorrelation time of the dynamic scattering medium was found to be $\tau_{\mathrm{c}} = 8.3$ ms by fitting $\alpha_{\mathrm{coef}}(t)$ with the function $\alpha_{\mathrm{coef}}(t) = A\exp\left(-2t/\tau_{\mathrm{c}}\right) + B$ (A and B are constants).

Here, the optical absorption of the guide star was switched between high and low states at a frequency of $f_{\mathrm{mod}} = 25$ Hz, corresponding to a switching period T_{GS} of 40 ms (Fig. 2b), which was much larger than the decorrelation time of the scattering medium. Holograms were recorded with a time interval of $1/(2f_{\mathrm{mod}}) = 20$ ms between adjacent holograms. Figure 2(c) shows the time-reversed foci with total cycle counts N of 1, 15, 45, and 80, respectively. Figure 2(d) shows that the PBR of the time-reversed focus increased rapidly and then plateaued. It can be seen that the PBR increases significantly (~25 times) from 7 to 173 when N increases from 1 to 80, which effectively proves the fast decorrelation suppression effect of PFS-DOPC.

Within the whole optical field $\mathbf{E}_{\mathrm{out}}$ of the scattered light exiting the scattering medium, the stable component $\mathbf{E}_{\mathrm{S}}$ should be large enough to guarantee a high-quality focus. As shown in Fig. 2b, the speckle correlation coefficient $\alpha_{\mathrm{coef}}(t)$ decreases rapidly due to the fast decorrelation component $\mathbf{E}_{\mathrm{D}}$, and then plateaus to a stable value due to $\mathbf{E}_{\mathrm{S}}$. Therefore, $\alpha_{\mathrm{coef}}(\infty)$ can be used to represent the percentage of $\mathbf{E}_{\mathrm{S}}$ in $\mathbf{E}_{\mathrm{out}}$. In addition, we simulated how $\alpha_{\mathrm{coef}}(\infty)$ could impact the maximum PBR that can be achieved by PFS-DOPC. The value of $\alpha_{\mathrm{coef}}(\infty)$ can be controlled by changing the size of the fast physiological motion

component. Figure 2(e) shows the PBR of the time-reversed focus as a function of the total cycle count N when $\alpha_{coef}(\infty)$ equals 0.18, 0.16, 0.14, and 0.10, respectively. Figure 2(f) shows that the maximum PBR obtained by the PFS-DOPC plateaus when $\alpha_{coef}(\infty)$ is greater than 0.18, while the maximum PBR is less than 2 when $\alpha_{coef}(\infty)$ is less than 0.08, where PFS-DOPC stops working.

Tissue-mimicking phantom experiments

To demonstrate the improvement of the light focusing inside dynamic scattering media by PFS-DOPC, we built an experimental setup, as shown in Fig. 3(a). A laser source (Verdi V5, Coherent, Inc.) with a wavelength of 532 nm was used to generate a collimated light beam. Then, the beam was split into a reference beam (reflected) and a sample beam (transmitted) by a polarizing beam splitter (PBS1) and a half-wave plate (HWP1). A half-wave plate (HWP2) was used to change the reference beam's polarization to -*p*-polariztion. To fully illuminate the aperture of the SLM (Pluto-2-VIS, Holoeye, Corp.), the diameter of the reference beam was expanded by L1 and L2. The sample beam was scattered when passing through a dynamic scattering medium and then collected by a lens L3. A beam splitter (BS1) was used to combine the reference beam and the sample beam. Then, their interference pattern was generated on the SLM's surface. A camera lens (CL) was installed on the camera (PCO.edge 5.5, PCO, Corp.) to image the interference pattern on the SLM plane for wavefront measurement. By changing the state of the guide star embedded inside the scattering medium for N cycles, $2N$ holograms were recorded by the camera and then a binary conjugated phase map was computed using Eq. (5). The SLM displayed the binary conjugated phase map and modulated the reference beam to focus light onto the guide star.

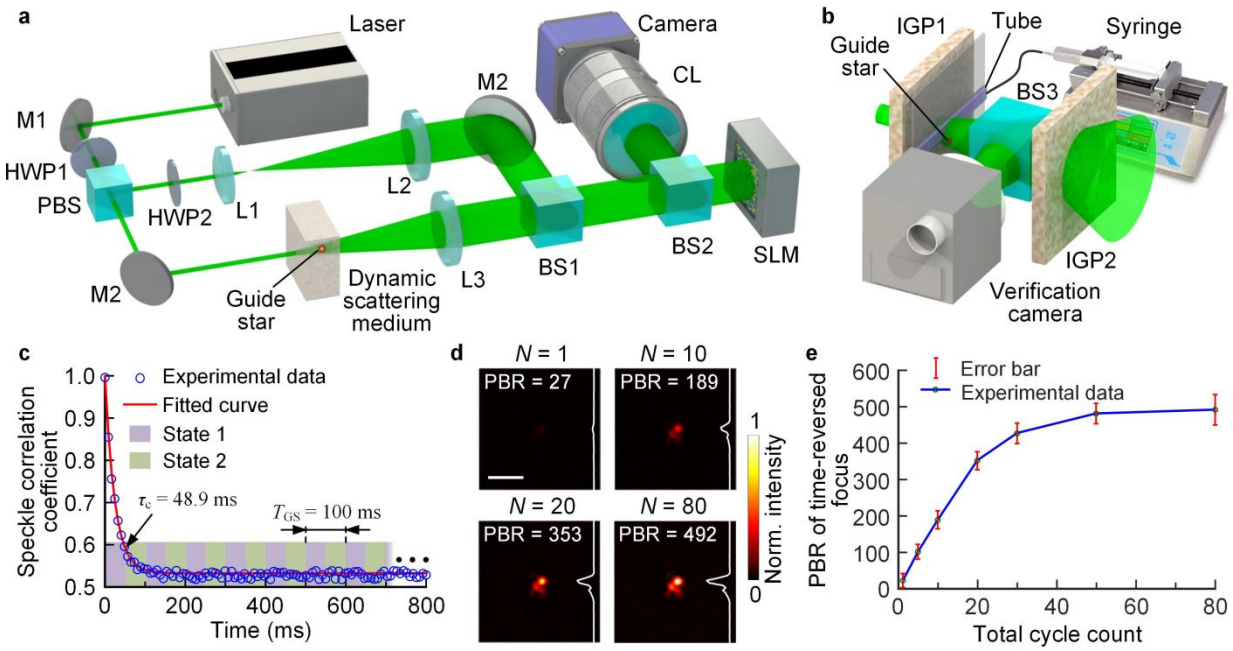

Figure 3. *In vitro* experiments for light focusing inside a dynamic scattering medium by PFS-DOPC. (a) Schematic illustration of the experimental setup. BS, beam splitter; CL, camera lens; HWP, half-wave plate; L, lens; M, mirror; PBS, polarizing beam splitter; SLM, spatial light modulator. (b) Setup for *in vitro* experiments. IGP, intralipid-gelatin phantom. (c) Speckle correlation coefficient as a function of time *t*. (d) Normalized (Norm.) intensity distribution of DOPC foci with total cycle count N = 1, 15, 45 and 125, respectively. Scale bar, 50 μm. (e) PBR of the experimental time-reversed focus as a function of the total cycle count N. Standard deviation over 10 datasets was indicated by the error bars.

An experimental setup was introduced to mimic a dynamic scattering medium and observe the focus inside it, as illustrated in Fig. 3(b). A glass-tube filled with 1% intralipid solution was sandwiched between two pieces of 1% intralipid-gelatin phantoms with a thickness of 1 mm (see Methods) to mimic a dynamic scattering medium. The intralipid solution inside the tube was driven by a syringe pump with a specific speed v_s to induce fast speckle decorrelation. By adjusting v_s, the decorrelation time of the dynamic scattering medium was controlled. Here, we controlled the decorrelation time to be 48.9 ms as shown in Fig. 3(c). To set a controllable guide star inside the scattering medium, a transmissive SLM (LC 2012, Holoeye, Corp.) was used to switch the polarization of the selected pixel. The guide star was switched between two different polarization states at a frequency of $f_{mod} = 10$ Hz. To observe the time-reversed focus, a verification camera was added on the conjugate plane of the guide star [Fig. 3(b)].

Figure 3(d) shows the time-reversed foci with total cycle counts N of 1, 10, 20, and 80. Figure 3(e) shows the PBR of the time-reversed focus as a function of N, which matches the trend of the angular-spectrum model well. The PBR increases 18 times from 27 to 492 when N increases from 1 to 80. This tissue-mimicking phantom experiment demonstrates that PFS-DOPC can significantly improve the light focusing quality inside dynamic scattering media.

Fighting against fast physiological motions *in vivo*

Next, we demonstrated the capability of PFS-DOPC to fight against fast physiological motions *in vivo* [Fig. 4(a)]. A guide star was sandwiched between a piece of intralipid-gelatin phantom (1% and 1-mm thickness) and a living-mouse ear (see Methods). No optical focus can be observed when light is directly focused through a living-mouse ear since the optical thickness of the mouse ear is ~17[33].

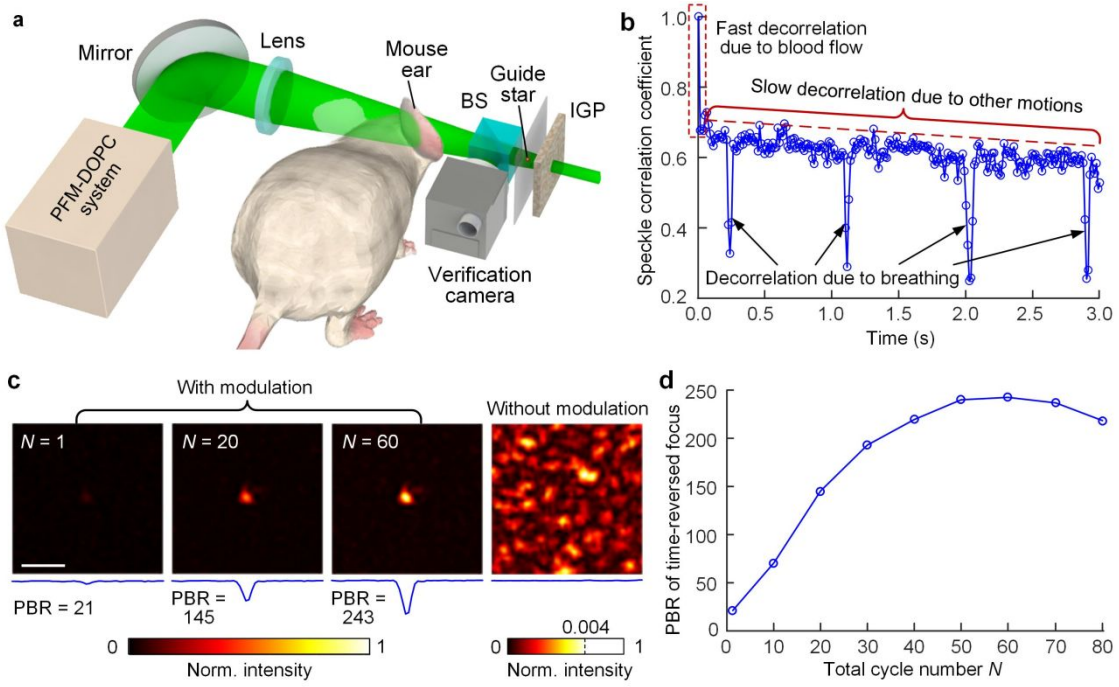

Figure 4. *In vivo* experiments of light focusing by PFS-DOPC. (a) Schematic illustration of the experimental setup. BS, beam splitter; IGP, intralipid-gelatin phantom. (b) Speckle correlation coefficient as a function of time t for a living-mouse ear. (c) Normalized (Norm.) intensity distribution of the time-reversed foci. Left, with guide star modulation for N = 1, 15, 45 and 125, respectively; Right, without guide star modulation. Scale bar, 100 μm. (d) PBR of the experimental time-reversed focus as a function of the total cycle count N.

As shown in Fig. 4(b), the decorrelation of the mouse ear was composed of fast decorrelation due to blood flow, periodic spike decorrelation due to breathing, and slow decorrelation due to other motions. Due to the fast decorrelation, the speckle correlation coefficient decreased from 1 to 0.68 within 12 ms, which presents the main challenge for efficiently tagging photons by a guide star *in vivo*.

Figure 4(c) shows the improvement of the PBR by PFS-DOPC with different total cycle numbers. The guide star was switched between two states at a frequency of $f_{\mathrm{mod}} = 10$ Hz. The PBR increased ~12 times from 21 to 243 when N increased from 1 to 60. No light focus was observed when the guide star modulation was off. The PBR of the time-reversed focus reaches the maximum when $N = 60$ and starts to decrease if $N > 60$ [Fig. 4(d)] because the slow decorrelation [Fig. 4(b)] starts to dominate with the increase of the overall DOPC time. The capability of PFS-DOPC to fight against fast physiological motions paves the way to realize high-quality light focusing in live tissue, especially when the speckle decorrelation time is less than 10 ms.

DISCUSSION

We have developed PFS-DOPC to combat fast physiological motions and achieved significantly improved light focusing quality inside dynamic scattering media. In PFS-DOPC, we modulated the guide star at a distinctive frequency for multiple cycles. Then the frequency of the tagged photons was shifted accordingly. In contrast, fast physiological motions, such as blood flow and respiration motions, perturbed photons randomly, thus those photons do not have a distinctive frequency shift. By detecting at the specific frequency, the tagged photons can be well separated from the randomly perturbed ones.

As demonstrations, we first simulated the performance of PFS-DOPC inside a dynamic scattering medium using the angular-spectrum method. As a result, a 25-fold enhancement of the PBR was obtained for the light focusing. Second, we conducted *in vivo* experiments in which we circulated intralipid solution to simulate the blood flow in live tissue. After a modulation of 80 cycles, the PBR increased 18 times compared with that of conventional DOPC. Finally, we demonstrated that PFS-DOPC can achieve 12-time PBR enhancement *in vivo*.

In addition to fighting against fast physiological motions, PFS-DOPC can also reduce the influence of environmental disturbances during the wavefront measurements, and thus it provides a robust solution for focusing light inside scattering media. For scattering media containing only fast decorrelation components, with the increase of the guide-star modulation cycle number, the PBR of the light focus increases and then plateaus. However, for live tissue, both fast and slow decorrelation exist. In this situation, the PBR of the light focus first grows and then decreases with the increase of the cycle number. Thus, there exists an optimal modulation cycle number to maximize the PBR *in vivo*.

In previous studies, the time-reversed ultrasonically encoded (TRUE) focusing technology used an ultrasonic focus as a guide star by shifting the frequency of the photons with the modulation of their phases[16,24,33]. The ultrasonically tagged photons were separated from the untagged ones during detection. However, the proposed PFS-DOPC method is a generalized approach that is applicable to various guide stars, including not only ultrasonic foci[16,24,33], but also kinetic targets[15,26], magnetic particles[28,29], photoswitchable proteins[34], and more, by modulating the guide stars at a distinctive frequency and employing frequency lock-in detection. In addition, the TRUE technology mainly focused on minimizing the system latency to beat fast speckle decorrelation[30,31] but did not provide sufficient focusing contrast due to the limited speeds of hardware. Our proposed PFS-DOPC method bypasses the hardware limit and offers a new approach to fighting against fast speckle decorrelation. Equipped with suitable guide stars in live tissue, PFS-DOPC may be exploited for new biomedical applications, such as microsurgery, photodynamic therapy, and optogenetics.

METHODS

Intralipid-gelatin phantom preparation. We made the intralipid-gelatin phantom from porcine skin gelatin (10% by weight, G2500-1kG, Sigma-Aldrich, USA), intralipid (20%, Fresenius Kabi, Sweden) and de-ionized water[35]. The reduced scattering coefficient μ_s' of the phantom was ~10 cm^{-1} by setting the lipid concentration as 1.5 g mL^{-1}. The thickness of the phantom was accurately controlled to be 1 mm by sandwiching acrylic spacers between two acrylic sheets.

Animal preparation. The mice used for *in vivo* experiments were adult female nude mice with 2- to 3-month-old (body weight: ~20−30 g; Hsd: Athymic Nude-FoxlNU, Harlan). 1.5% vaporized isoflurane was used to maintain the mouse under anesthesia in experiments. A lab-made animal holder was used to tape the anesthetized mouse. All experiments were carried out under laboratory animal protocols (Wang lab 1737) permitted by the Institutional Animal Care and Use Committee at California Institute of Technology.

SUPPORTING INFORMATION

Supporting Information is available from the Online Library or from the author.

DATA AVAILABILITY

The data that support the findings of this study are available from the corresponding authors upon reasonable request.

ACKNOWLEDGEMENTS

This work was financially supported by the National Institutes of Health (NIH) grants CA186567 (NIH Director's Transformative Research Award), NS090579 and NS099717.

COMPETING FINANCIAL INTERESTS

L. V. Wang has a financial interest in Microphotoacoustics, Inc., CalPACT, LLC, and Union Photoacoustic Technologies, Ltd., which, however, did not support this work. The other authors declare no competing financial interests.

REFERENCES

(1) Choi, Y.; Yang, T. D.; Fang-Yen, C.; Kang, P.; Lee, K. J.; Dasari, R. R.; Feld, M. S.; Choi, W. Overcoming the diffraction limit using multiple light scattering in a highly disordered medium. *Physical Review Letters* 2011, *107* (2), 023902.

(2) Mounaix, M.; Andreoli, D.; Defienne, H.; Volpe, G.; Katz, O.; Grésillon, S.; Gigan, S. Spatiotemporal coherent control of light through a multiple scattering medium with the multispectral transmission matrix. *Physical Review Letters* 2016, *116* (25), 253901.

(3) Popoff, S. M.; Lerosey, G.; Carminati, R.; Fink, M.; Boccara, A. C.; Gigan, S. Measuring the Transmission Matrix in Optics: An approach to the study and control of light propagation in disordered media. *Physical Review Letters* 2010, *104* (10), 100601.

(4) Boniface, A.; Mounaix, M.; Blochet, B.; Piestun, R.; Gigan, S. Transmission-matrix-based point-spread-function engineering through a complex medium. *Optica* 2017, *4* (1), 54.
(5) Vellekoop, I. M.; Mosk, A. P. Focusing coherent light through opaque strongly scattering media. *Optics Letters* 2007, *32* (16), 2309–2311.
(6) Conkey, D. B.; Caravaca-Aguirre, A. M.; Piestun, R. High-Speed scattering medium characterization with application to focusing light through turbid media. *Optics express* 2012, *20* (2), 1733–1740.
(7) Lai, P.; Wang, L.; Tay, J. W.; Wang, L. V. Photoacoustically guided wavefront shaping for enhanced optical focusing in scattering media. *Nature Photonics* 2015, *9* (2), 126–132.
(8) Tzang, O.; Niv, E.; Singh, S.; Labouesse, S.; Myatt, G.; Piestun, R. Wavefront shaping in complex media with a 350 khz modulator via a 1D-to-2D Transform. *Nat. Photonics* 2019, 1–6.
(9) Hsieh, C.-L.; Pu, Y.; Grange, R.; Psaltis, D. Digital phase conjugation of second harmonic radiation emitted by nanoparticles in turbid media. *Optics Express* 2010, *18* (12), 12283.
(10) Wang, D.; Zhou, E. H.; Brake, J.; Ruan, H.; Jang, M.; Yang, C. Focusing through dynamic tissue with millisecond digital optical phase conjugation. *Optica* 2015, *2* (8), 728–735.
(11) Cui, M.; Yang, C. Implementation of a digital optical phase conjugation system and its application to study the robustness of turbidity suppression by phase conjugation. *Optics Express* 2010, *18* (4), 3444.
(12) Yang, J.; Shen, Y.; Liu, Y.; Hemphill, A. S.; Wang, L. V. Focusing light through scattering media by polarization modulation based generalized digital optical phase conjugation. *Applied Physics Letters* 2017, *111* (20), 201108.
(13) Papadopoulos, I. N.; Farahi, S.; Moser, C.; Psaltis, D. Focusing and scanning light through a multimode optical fiber using digital phase conjugation. *Optics Express* 2012, *20* (10), 10583.
(14) Tripathi, S.; Paxman, R.; Bifano, T.; Toussaint, K. C. Vector transmission matrix for the polarization behavior of light propagation in highly scattering media. *Optics Express* 2012, *20* (14), 16067.
(15) Ma, C.; Xu, X.; Liu, Y.; Wang, L. V. Time-reversed adapted-perturbation (TRAP) optical focusing onto dynamic objects inside scattering media. *Nature Photonics* 2014, *8* (12), 931–936.
(16) Wang, Y. M.; Judkewitz, B.; DiMarzio, C. A.; Yang, C. Deep-tissue focal fluorescence imaging with digitally time-reversed ultrasound-encoded light. *Nature Communications* 2012, *3* (1), 928.
(17) Si, K.; Fiolka, R.; Cui, M. Fluorescence imaging beyond the ballistic regime by ultrasound-pulse-guided digital phase conjugation. *Nature Photonics* 2012, *6* (10), 657–661.
(18) Hillman, T. R.; Yamauchi, T.; Choi, W.; Dasari, R. R.; Feld, M. S.; Park, Y.; Yaqoob, Z. Digital optical phase conjugation for delivering two-dimensional images through turbid media. *Scientific Reports* 2013, *3* (1), 1909.
(19) Judkewitz, B.; Wang, Y. M.; Horstmeyer, R.; Mathy, A.; Yang, C. Speckle-scale focusing in the diffusive regime with time reversal of variance-encoded light (TROVE). *Nature Photonics* 2013, *7* (4), 300–305.
(20) Park, J.; Park, J.-H.; Yu, H.; Park, Y. Focusing through turbid media by polarization modulation. *Optics Letters* 2015, *40* (8), 1667.
(21) Yang, J.; Li, J.; He, S.; Wang, L. V. Angular-spectrum modeling of focusing light inside scattering media by optical phase conjugation. *Optica* 2019, *6* (3), 250.
(22) Vellekoop, I. M.; Cui, M.; Yang, C. Digital optical phase conjugation of fluorescence in turbid tissue. *Applied Physics Letters* 2012, *101* (8), 081108.
(23) Kong, L.; Cui, M. In vivo fluorescence microscopy via iterative multi-photon adaptive compensation technique. *Optics express* 2014, *22* (20), 23786–23794.
(24) Xu, X.; Liu, H.; Wang, L. V. Time-reversed ultrasonically encoded optical focusing into scattering media. *Nature Photonics* 2011, *5* (3), 154–157.
(25) Ruan, H.; Brake, J.; Robinson, J. E.; Liu, Y.; Jang, M.; Xiao, C.; Zhou, C.; Gradinaru, V.; Yang, C. Deep tissue optical focusing and optogenetic modulation with time-reversed ultrasonically encoded light. *Science Advances* 2017, *3* (12), eaao5520.
(26) Zhou, E. H.; Ruan, H.; Yang, C.; Judkewitz, B. Focusing on moving targets through scattering

samples. *Optica* 2014, *1* (4), 227–232.
(27) Ruan, H.; Jang, M.; Yang, C. Optical focusing inside scattering media with time-reversed ultrasound microbubble encoded light. *Nat Commun* 2015, *6*, 8968.
(28) Ruan, H.; Haber, T.; Liu, Y.; Brake, J.; Kim, J.; Berlin, J. M.; Yang, C. Focusing light inside scattering media with magnetic-particle-guided wavefront shaping. *Optica* 2017, *4* (11), 1337.
(29) Yu, Z.; Huangfu, J.; Zhao, F.; Xia, M.; Wu, X.; Niu, X.; Li, D.; Lai, P.; Wang, D. Time-reversed magnetically controlled perturbation (trmcp) optical focusing inside scattering media. *Scientific Reports* 2018, *8* (1), 2927.
(30) Liu, Y.; Ma, C.; Shen, Y.; Shi, J.; Wang, L. V. Focusing light inside dynamic scattering media with millisecond digital optical phase conjugation. *Optica* 2017, *4* (2), 280–288.
(31) Liu, Y.; Ma, C.; Shen, Y.; Wang, L. V. Bit-efficient, sub-millisecond wavefront measurement using a lock-in camera for time-reversal based optical focusing inside scattering media. *Opt. Lett.* 2016, *41* (7), 1321–1324.
(32) Ma, C.; Zhou, F.; Liu, Y.; Wang, L. V. Single-exposure optical focusing inside scattering media using binarized time-reversed adapted perturbation. *Optica* 2015, *2* (10), 869–876.
(33) Liu, Y.; Lai, P.; Ma, C.; Xu, X.; Grabar, A. A.; Wang, L. V. Optical focusing deep inside dynamic scattering media with near-infrared time-reversed ultrasonically encoded (TRUE) light. *Nature communications* 2015, *6*, 5904.
(34) Yang, J.; Li, L.; Shemetov, A. A.; Lee, S.; Zhao, Y.; Liu, Y.; Shen, Y.; Li, J.; Oka, Y.; Verkhusha, V. V.; et al. Focusing light inside live tissue using reversibly switchable bacterial phytochrome as a genetically encoded photochromic guide star. *Science Advances* 2019, *5* (12), eaay1211.
(35) Lai, P.; Xu, X.; Wang, L. V. Dependence of optical scattering from intralipid in gelatin-gel based tissue-mimicking phantoms on mixing temperature and time. *Journal of Biomedical Optics* 2014, *19* (3), 035002.

For Table of Contents Use Only

Fighting against fast speckle decorrelation for light focusing inside live tissue by photon frequency shifting

Jiamiao Yang, Lei Li, Jingwei Li, Zhongtao Cheng, Yan Liu, and Lihong V. Wang

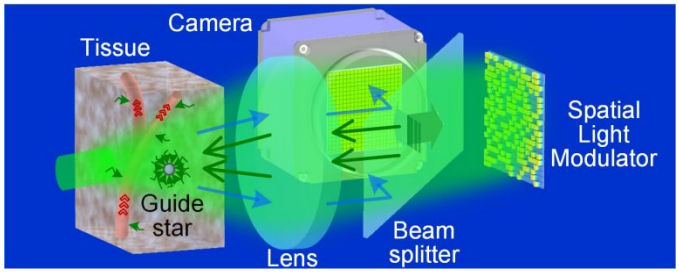

Brief synopsis: PSF-DOPC method is proposed to fight against fast physiological motions and focus light inside dynamic scattering media.